Electronic Structure, Phonon Dynamical Properties, and CO_2 Capture Capability of $Na_{2-x}M_xZrO_3$ (M = Li,K): Density-Functional Calculations and Experimental Validations

Yuhua Duan,[1,*] Jonathan Lekse,[1] Xianfeng Wang,[1,2] Bingyun Li,[1,2] Brenda Alcántar-Vázquez,[3] Heriberto Pfeiffer,[3] and J. W. Halley[4]

[1]*National Energy Technology Laboratory, U.S. Department of Energy, Pittsburgh, Pennsylvania 15236, USA*

[2]*School of Medicine, West Virginia University, Morgantown, West Virginia 26506, USA*

[3]*Instituto de Investigaciones en Materiales, Universidad Nacional Autónoma de México, Circuito Exterior s/n, Ciudad Universitaria, Delegación Coyoacan, Código Postal 04510, México Distrito Federal, Mexico*

[4]*School of Physics and Astronomy, University of Minnesota, Minneapolis, Minnesota 55455, USA*

(Received 11 December 2014; revised manuscript received 3 March 2015; published 22 April 2015)

The electronic structural and phonon properties of $Na_{2-\alpha}M_\alpha ZrO_3$ (M = Li,K, α = 0.0,0.5,1.0,1.5,2.0) are investigated by first-principles density-functional theory and phonon dynamics. The thermodynamic properties of CO_2 absorption and desorption in these materials are also analyzed. With increasing doping level α, the binding energies of $Na_{2-\alpha}Li_\alpha ZrO_3$ are increased while the binding energies of $Na_{2-\alpha}K_\alpha ZrO_3$ are decreased to destabilize the structures. The calculated band structures and density of states also show that, at the same doping level, the doping sites play a significant role in the electronic properties. The phonon dispersion results show that few soft modes are found in several doped configurations, which indicates that these structures are less stable than other configurations with different doping levels. From the calculated relationships among the chemical-potential change, the CO_2 pressure, and the temperature of the CO_2 capture reactions by $Na_{2-\alpha}M_\alpha ZrO_3$, and from thermogravimetric-analysis experimental measurements, the Li- and K-doped mixtures $Na_{2-\alpha}M_\alpha ZrO_3$ have lower turnover temperatures (T_t) and higher CO_2 capture capacities, compared to pure Na_2ZrO_3. The Li-doped systems have a larger T_t decrease than the K-doped systems. When increasing the Li-doping level α, the T_t of the corresponding mixture $Na_{2-\alpha}Li_\alpha ZrO_3$ decreases further to a low-temperature range. However, in the case of K-doped systems $Na_{2-\alpha}K_\alpha ZrO_3$, although doping K into Na_2ZrO_3 initially shifts its T_t to lower temperatures, further increases of the K-doping level α causes T_t to increase. Therefore, doping Li into Na_2ZrO_3 has a larger influence on its CO_2 capture performance than the K-doped Na_2ZrO_3. Compared with pure solids M_2ZrO_3, after doping with other elements, these doped systems' CO_2 capture performances are improved.

DOI: 10.1103/PhysRevApplied.3.044013

I. INTRODUCTION

The burning of fossil fuels is still the main energy source for the world's economy. One consequence of the use of these fuels is the emission of huge quantities of CO_2 into the atmosphere, creating environmental problems such as global climate change [1–3]. To solve such problems, there is a need to reduce CO_2 emissions into the atmosphere through capture and sequestration [4–6].

For a given CO_2 capture technology, the optimal working conditions [CO_2 pressures of pre- and postcapture, absorption-desorption temperature range (ΔT_O), etc.] are fixed. However, at a given CO_2 pressure, the turnover temperature (T_t) of an individual solid capture CO_2 reaction is fixed. The T_t may be outside the operating temperature range ΔT_O for a particular capture technology. In order to adjust T_t to fit the practical working ΔT_O through reversible chemical transformations, we demonstrate that, by mixing different types of solids, it is possible to shift T_t to the practical operating ΔT_O range [7–9]. Generally, when we mix two solids A and B to form a new sorbent C, the turnover temperature of the newly resulting system (T_C) is located between those temperatures of A and B (T_A, T_B), assuming that A is a strong CO_2 sorbent while B is a weak CO_2 sorbent, and $T_A > T_B$. Also, we assume that the desired operating temperature (T_O) is between T_A and T_B ($T_A > T_O > T_B$). Depending on the properties of A and B, we typically have three scenarios to synthesize the mixing sorbent C:

(a) $T_A \gg T_B$ and the A component is the key component for capturing CO_2. In this case, since T_A is higher than T_O, mixing B into A will decrease the turnover T_C of the C solid to values closer to T_O. For example, Li_2O

*To whom all correspondence should be addressed. yuhua.duan@netl.doe.gov

 © 2015 American Physical Society

is a very strong CO_2 sorbent which forms Li_2CO_3. However, its regeneration from Li_2CO_3 only can occur at very high temperature (T_A). In order to move its T_A to lower temperatures, one can mix in some weak CO_2 sorbents (such as SiO_2 or ZrO_2). Our results show that, in this way, the turnover T_t and the theoretical CO_2 capture capacity of mixtures decrease as the ratios of $Li_2O:SiO_2$ or $Li_2O:ZrO_2$ decrease [7–13].

(b) $T_A \gg T_B$ and the B component is the key component for capturing CO_2. In this case, since T_B is lower than T_O, mixing A into B will increase the turnover temperature T_C of the C solid to values closer to T_O. For example, pure MgO (as the B component) has a very high theoretical CO_2 capture capacity [14]. However, its T_B (250 °C) is lower than the required temperature range of 300–470 °C used in warm-gas cleanup technology, its practical CO_2 capacity is very low, and therefore, it cannot be used directly as a CO_2 sorbent in this technology. Our experimental and theoretical results show that by mixing alkali-metal oxides M_2O ($M = \mathrm{Na,K,Cs,Ca}$) or carbonates (M_2CO_3) into MgO, the newly formed mixed systems have higher turnover temperatures, making them useful as CO_2 sorbents through the reaction $MgO + CO_2 + M_2CO_3 = M_2Mg(CO_3)_2$ [15–17].

(c) Both A and B components are active for capturing CO_2. In this case, the CO_2 capacity of the mixture is the summation of those capacities of A and B. Li_2MSiO_4 ($M = \mathrm{Mg,Ca}$, etc.) and $M_{2-a}N_aZrO_3$ ($M, N = \mathrm{Li,Na,K}$) belong to this category. Obviously, those doped systems can be treated as mixing of three solids ($Li_2O:MO:SiO_2$, $M_2O:N_2O:ZrO_2$). In this study, we focus on this type of mixing sorbents: $Na_{2-\alpha}M_\alpha ZrO_3$ ($M = \mathrm{Li,Na,K}$, $\alpha = 0,0.5,1.0,1.5,2.0$).

During past decades, experimental investigations widely found that the alkali-metal zirconates are good candidates for CO_2 capture because of their a large CO_2-sorption capacity, an infinite CO_2-N_2 or CO_2-H_2 selectivity, good reversibility, and high operating temperatures [4,18–33]. Nakagawa and Ohashi [19,20] first reported that lithium zirconate powder reacts immediately with ambient CO_2 in the range of 450 °C to 550 °C and that the products react and return reversibly to lithium zirconate at temperatures above 650 °C. Recent experimental results also indicate that doping or mixing another alkali-metal salt into lithium zirconate can improve the CO_2 sorption [29,30,34]. With a thermal gravimetric analyzer under isothermal conditions, Fauth and co-workers [25] conclude that the combination of binary alkali carbonate, binary alkali-metal–alkaline-earth-metal carbonate, ternary alkali-metal carbonate, and ternary alkali-metal-carbonate–halide eutectics with Li_2ZrO_3 noticeably improves the CO_2 uptake rate and the CO_2-sorption capacity. These results are confirmed by Pannocchia and co-workers [18]. Lopez-Ortiz and co-workers [35] find that Na_2ZrO_3 presents better CO_2 sorption than Li_2ZrO_3. Pfeiffer and co-workers [29,30,34] demonstrate that the lithium-sodium and lithium-potassium metazirconates ($Li_{2-x}M_xZrO_3$, $M = \mathrm{Na,K}$, $0 \le x \le 2$) present better CO_2 absorption than pure Li_2ZrO_3. Ochoa-Fernandez and co-workers [36] demonstrate that both the capture rate and capacity of lithium zirconate depend strongly on the ratio of Li_2O to ZrO_2. Enhanced capture rates are observed when there is less Li_2O than ZrO_2, possibly because excess ZrO_2 acts as a dispersant and introduces more reactive boundaries. The recent investigation on the effects of steam addition on the stability of Li_2ZrO_3 capture of CO_2 shows that the presence of steam enhances the capture and regeneration rates but results in a large decay in the CO_2 capacity, compared with capture under dry conditions [37]. Sandoval-Díaz and Pfeiffer [38] explore the effects of CO_2 chemisorption on K-doped Na_2ZrO_3 and they find that K doping enhances the CO_2 chemisorption and diffusion kinetics of Na_2ZrO_3 and that a 40% doping rate gives the best solid solution for the CO_2 capture. Velderrain and co-workers [39] find that a small portion of Li addition increases the absorption capacity of Na_2ZrO_3, but too much Li (>25% mol) decreases its absorption capacity. From thermodynamic calculations and experimental measurements, Nakagawa and Ohashi [20] point out that the difference in CO_2 sorption capacity between Li_2ZrO_3 and ZrO_2 not only depends on temperature and the CO_2 partial pressure but also on the presence of molten carbonates, e.g. an alkali-metal carbonate molar ratio of $\mathrm{Li:K} = 62:38$.

Computational modeling is one of the more useful tools to identify CO_2 sorbent candidates with optimal performance [7,8,10–12,14]. Our previous results on Li_2ZrO_3 and $Li_6Zr_2O_7$ capturing CO_2 show that the CO_2 capture performance of Li_2ZrO_3 is better than that of $Li_6Zr_2O_7$ and therefore there is no advantage to using $Li_6Zr_2O_7$ as a CO_2 sorbent [10]. For M_2ZrO_3 ($M = \mathrm{Li,Na,K}$), our previous results demonstrate that Na_2ZrO_3 has a CO_2 capture performance similar to that of Li_2ZrO_3, while K_2ZrO_3 is not a good CO_2-sorbent candidate because it can only be regenerated at very high temperatures [11]. When substituting half of Li in Li_2ZrO_3 with Na or K, we find that the newly formed $LiNaZrO_3$ has a lower T_t, compared to pure Li_2ZrO_3, while $LiKZrO_3$ has a bit higher T_t [40]. In this study, continuing the previous investigation, we first build our doped systems by substituting a portion of the Na in Na_2ZrO_3 with Li or K in different $\mathrm{Na:Li}$ and $\mathrm{Na:K}$ ratios. Then, by combining a first-principles density-functional method with phonon dynamics, we extensively investigate the electronic structural and the lattice dynamical phonon properties of pure and doped $Na_{2-\alpha}M_\alpha ZrO_3$ ($M = \mathrm{Li,K}$, $\alpha = 0.0,0.5,1.0,1.5,2.0$) systems. Based on the calculated energetic and thermodynamic results, the CO_2 absorption and desorption properties of these doped lithium zirconates are analyzed in detail. The obtained results provide a deeper understanding of the effects of compositional

changes on the CO_2 capture performance of mixed sorbents and further facilitate the development of CO_2 sorbents that will be vital to solving global climate-change problems associated with fossil-fuel usage.

The remaining sections of this paper are organized as follows: in Secs. II and III, we briefly describe the theoretical and experimental methods we employ. In Sec. IV, we present the electronic and phonon results for these pure and doped $Na_{2-\alpha}M_\alpha ZrO_3$ systems and compare them with other available data. This is followed by analysis of their capabilities for CO_2 capture by calculating the chemical-potential change for the capture reactions under different CO_2 pressure and temperature regimes. In Sec. V, we summarize our conclusions.

II. THEORETICAL METHODS

The calculation performed in this work is based on first-principles density-functional theory (DFT) with plane-wave basis sets and pseudopotentials to describe the electron-ion interactions. The Vienna *ab initio* simulation package (VASP) [41,42] is employed in this study to calculate the electronic structures of the lithium zirconates and zirconia materials. All calculations are done using the projector-augmented-wave (PAW) pseudopotentials and the Perdew-Wang 1991 exchange-correlation functional [43]. This computational level is shown to provide an accurate description for oxide systems [44]. Plane-wave basis sets are used with a plane-wave cutoff energy of 500 eV and a kinetic energy cutoff for augmentation charges of 605.4 eV. The k-point sampling grids of $7 \times 4 \times 4$, obtained by the Monkhorst-Pack method [45], are used for these bulk calculations. The valence electrons contain s and p orbitals for M (M = Li,Na,K) and O atoms, and s, p, and d orbitals for Zr. During calculations, all atoms in the cell as well as the lattice dimensions and angles are relaxed to the equilibrium configurations. For the band structure and phonon dispersion calculations, the symbols and coordinates of the high-symmetrical points in the first Brillouin zone of the crystals are taken from Bradley and Cracknell's definitions [46].

Detailed descriptions of our computational methodology can be found in our previous publications [8–14,47]. Here, we limit ourselves to providing only the main aspects relevant for the current study. The CO_2 capture reactions for pure and mixed alkali-metal zirconates $Na_{2-\alpha}M_\alpha ZrO_3$ can be expressed generically in the form (for convenience in description, we normalize the reaction to 1 mol of CO_2)

$$\mathrm{Na}_{2-\alpha}M_\alpha\mathrm{ZrO}_3 + \mathrm{CO}_2 \leftrightarrow \frac{2-\alpha}{2}\mathrm{Na}_2\mathrm{CO}_3 + \frac{\alpha}{2}M_2\mathrm{CO}_3 + \mathrm{ZrO}_2$$
$$(M = \mathrm{Li,K}; \alpha = 0, 0.5, 1.0, 1.5, 2.0).$$

Assuming that the difference between the chemical potential ($\Delta\mu^0$) of the solid phases can be approximated by the differences in their electronic energy (ΔE^{DFT}), their entropies (ΔS^{ph}), and their harmonic free energies (ΔF^{ph}), we can obtain the temperature- and pressure-dependent chemical-potential change ($\Delta\mu$) for these reactions [8,13,14,48,49],

$$\Delta\mu(T,P) = \Delta\mu^0(T) - RT\ln\frac{P_{\mathrm{CO}_2}}{P_0}, \tag{1}$$

with

$$\Delta\mu^0(T) \approx \Delta E^{\mathrm{DFT}} + \Delta E_{\mathrm{ZP}} + \Delta F^{\mathrm{ph}}(T) - G_{\mathrm{CO}_2}(T), \tag{2}$$

where $\Delta\mu^0(T)$ is the standard Gibbs free-energy change of the reaction, ΔE_{ZP} is the zero-point energy difference between the reactants and products that can be obtained directly from phonon calculations. P_0 is the standard state reference pressure of 1 bar. The free energy and entropy of CO_2 (G_{CO_2}, S_{CO_2}) can be obtained with standard statistical mechanics [50].

In the harmonic approximation, the phonon free-energy change (ΔF^{ph}) and the entropy change (ΔS^{ph}) between the solid reactants and products can be calculated based on the Helmholtz free energy of the solids F_{harm} and the entropy of the solids (S_{harm})

$$\Delta F^{\mathrm{ph}}(T) = \sum_{\text{solid products}} F_{\mathrm{harm}}(T) - \sum_{\text{solid reactants}} F_{\mathrm{harm}}(T), \tag{3}$$

$$\Delta S^{\mathrm{ph}}(T) = \sum_{\text{solid products}} S_{\mathrm{harm}}(T) - \sum_{\text{solid reactants}} S_{\mathrm{harm}}(T), \tag{4}$$

where the F_{harm}, S_{harm}, and the total vibrational (phonon) energy (E_{tot}) of the solids are defined as [51]

$$F_{\mathrm{harm}} = rk_BT\int_0^\infty g(\omega)\ln\left[2\sinh\left(\frac{\hbar\omega}{2k_BT}\right)\right]d\omega, \tag{5}$$

$$S_{\mathrm{harm}} = rk_B\int_0^\infty g(\omega)\left\{\left(\frac{\hbar\omega}{2k_BT}\right)\left[\coth\left(\frac{\hbar\omega}{2k_BT}\right) - 1\right] - \ln[1 - e^{-(\hbar\omega/2k_BT)}]\right\}d\omega, \tag{6}$$

$$E_{\mathrm{tot}} = \frac{1}{2}r\int_0^\infty g(\omega)(\hbar\omega)\coth\left(\frac{\hbar\omega}{2k_BT}\right)d\omega. \tag{7}$$

In Eqs. (5), (6), and (7), r is the number of degrees of freedom in the primitive unit cell, ω is the phonon dispersion frequency, and $g(\omega)$ is the phonon density of states. It can be seen that the zero-point-energy (E_{ZP}) can be obtained from Eq. (7) by taking $T \to 0$,

$$E_{\mathrm{ZP}} = \lim_{T\to 0}[E_{\mathrm{tot}}(T)]. \tag{8}$$

The enthalpy changes [$\Delta H^{\mathrm{cal}}(T)$] for the capture reactions above Eq. (1) can be derived from Eqs. (2), (3), (4), (5), and (6)) as

$$\Delta H^{\mathrm{cal}}(T) = \Delta\mu^0(T) + T[\Delta S^{\mathrm{ph}}(T) - S_{\mathrm{CO_2}}(T)]. \quad (9)$$

In this study, we employed the PHONON software package [52] in which the direct method is applied following the formula derived by Parlinski, Li, and Kawazoe [53] to combine the *ab initio* DFT with phonon calculations. Similar to our previous approach, the phonon dispersion and the thermodynamic properties (zero-point energy, free-energy change, and entropy change, etc.) can be found for each crystal. In turn, the zero-point energy change (ΔE_{ZP}) and the phonon free-energy change [$\Delta F^{\mathrm{ph}}(T)$ in Eq. (2)] are obtained for the CO_2 capture reactions.

In the phonon calculations, a $2 \times 1 \times 1$ supercell is created for $Na_{2-\alpha}M_\alpha ZrO_3$ from their optimized unit cells, which are calculated through DFT. A displacement of 0.03 Å of nonequivalent atoms is generated. Then for the supercell, the DFT calculations are performed again to obtain the force on each atom due to the displacements. These forces are carried back to the PHONON package [52] to calculate the phonon dispersions and densities. Partition functions constructed from the phonon dispersions and densities are employed to calculate the thermodynamic properties, such as internal energy, free energy, entropy, heat capacity, etc. These thermodynamic properties are evaluated at various temperatures and CO_2 pressures, with the use of Eq. (1) to calculate the chemical-potential changes for the capture reactions given above Eq. (1) [8–14].

III. EXPERIMENTAL MEASUREMENTS

The Li- and K-doped Na_2ZrO_3 samples are synthesized by a solid-state reaction. These compositions are selected based on our theoretical results obtained in this work. The initial reagents are used as obtained: (a) sodium carbonate, anhydrous, 99.5%, Alfa Aesar; (b) potassium carbonate, anhydrous, 99%, Alfa Aesar; (c) lithium carbonate, anhydrous, 99% Alfa Aesar; (d) zirconium(IV) oxide, 99%, Sigma-Aldrich. The Na_2ZrO_3, $Na_{2-\alpha}Li_\alpha ZrO_3$, and $Na_{2-\alpha}K_\alpha ZrO_3$ are synthesized from stoichiometric mixtures of Na_2CO_3, K_2CO_3, Li_2CO_3, and ZrO_2. The corresponding mixtures are ground in an agate mortar by hand for 10 min and then transferred to an alumina crucible. The crucible is placed into a box furnace and heated at 900 °C for 4 h. The samples are rapidly cooled to room temperature and then ground by hand for 10 min in an agate mortar prior to physical-property measurements. Correct stoichiometry of the products is assured based on the ratio of the starting materials.

A Panalytical X'Pert Pro diffractometer is used to collect powder diffraction patterns for the obtained samples. Scans are performed from $2\theta = 5°$–$100°$, with a step size of 0.17° and a scan speed of 200 s/deg. The patterns are analyzed using Panalytical's Highscore Plus to determine the compositions of samples in this study.

A PerkinElmer Lambda 1050 dual-beam spectrometer is used to collect data for each compound from 200 to 2500 nm. The Kubelka-Munk equation [54] is then used to convert reflectance data into absorbance data for analysis. Band-gap values are then determined using a standard method in which the absorption edge is extrapolated to zero.

Experimental CO_2 capture studies are conducted using thermogravimetric analysis (TGA). Data are collected on a Mettler Toledo differential scanning calorimeter (DSC). For analysis, a sample of approximately 50 mg is heated from 30 to 800 °C, followed by a dwell of 30 min at 800 °C, under flowing carbon dioxide gas (75 ml/min).

Table S1 of the Supplemental Material [55] summarizes the experimental details and the measured data.

IV. RESULTS AND DISCUSSIONS

A. Theoretical structural optimization

As described in Sec. III, the alkali-metal zirconates can be synthesized from alkali carbonates and ZrO_2 with different ratios [56–58]. As Bastow and co-workers [56] measured, the structure of Na_2ZrO_3 is isostructural with Li_2SnO_3 [59] and Li_2TiO_3 [60,61] crystallizing in a monoclinic space group $C2/c$ (no. 15) with unit-cell parameters $a = 5.623$ Å, $b = 9.749$ Å, $c = 11.127$ Å, and $\beta = 99.98°$, and with eight formula units (f.u.) per unit cell. As shown in Fig. 1, in Na_2ZrO_3, there are three types of Na which can be substituted by M (M = Li,K) with different Na:M ratios α to form $Na_{2-\alpha}M_\alpha ZrO_3$. In order to keep the symmetry unchanged, at each ratio α, two possible substitution systems ($Na_{2-\alpha}M_\alpha ZrO_3$-$A$ and $Na_{2-\alpha}M_\alpha ZrO_3$-$B$) are created. The optimized structural constants of these substituted systems are summarized in Table I.

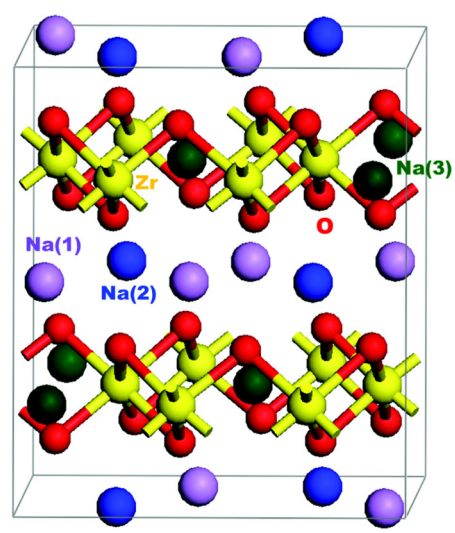

FIG. 1. The crystal structure of Na_2ZrO_3. The c axis is vertical. There are three types of Na atoms in the structure. By substituting these Na with M (M = Li,K) under different combinations, two types (A, B) of $Na_{2-\alpha}M_\alpha ZrO_3$ (α = 0.0,0.5,1.0,1.5,2.0) are obtained.

TABLE I. The optimized crystal-structure constants and atomic fractional coordinates of pure and doped zirconates, $Na_{2-\alpha}M_{\alpha}ZrO_3$ (M = Li,K).

Crystal and space group	Optimized lattice constants		Optimized fractional coordinates	
	Case *A*	Case *B*	Case *A*	Case *B*
$\alpha = 0.0$	Experimental:	Optimized:	Experimental:	Optimized:
Na_2ZrO_3	$a = 5.623$ Å	$a = 5.612\,809$ Å	Na: (0.238, 0.077, −0.0001)	Na: (0.236 47, 0.078 72, −0.000 24)
$C12/c1$ (no. 15)[a]	$b = 9.749$ Å	$b = 9.735\,747$ Å	(0.250, 0.250, 0.500)	(0.250 00, 0.250 00, 0.500 00)
	$c = 11.127$ Å	$c = 10.956\,75$ Å	(0.000, 0.085, 0.250)	(0.000 00, 0.084 84, 0.250 00)
	$\beta = 99.98°$	$\beta = 100.01°$	Zr: (0.000, 0.415, 0.250)	Zr: (0.000 00, 0.417 92, 0.250 00)
	$V = 600.74$ Å^3	$V = 617.806$ Å^3	(0.000, 0.747, 0.250)	(0.000 00, 0.750 26, 0.250 00)
			O: (0.141, 0.265, 0.138)	O: (0.147 31, 0.268 49, 0.142 48)
			(0.102, 0.586, 0.138)	(0.096 80, 0.584 61, 0.142 22)
			(0.138, 0.906, 0.135)	(0.145 91, 0.901 65, 0.140 87)
$\alpha = 0.5$	$a = 5.598\,09$ Å	$a = 5.527\,29$ Å	Li: (0.250 00, 0.250 00, 0.500 00)	Li: (0.000 00, 0.083 89, 0.250 00)
$Na_{1.5}Li_{0.5}ZrO_3$	$b = 9.704\,63$ Å	$b = 9.584\,52$ Å	Na: (0.234 83, 0.077 89, −0.000 28)	Na: (0.235 26, 0.078 42, −0.000 19)
	$c = 10.681\,59$ Å	$c = 10.921\,61$ Å	(0.000 00, 0.074 27, 0.250 00)	(0.250 00, 0.250 00, 0.500 00)
	$\beta = 99.45°$	$\beta = 99.76°$	Zr: (0.000 00, 0.405 67, 0.250 00)	Zr: (0.000 00, 0.416 48, 0.250 00)
	$V = 572.429$ Å^3	$V = 570.212$ Å^3	(0.000 00, 0.738 60, 0.250 00)	(0.000 00, 0.748 94, 0.250 00)
			O: (0.148 99, 0.258 29, 0.139 79)	O: (0.141 36, 0.260 50, 0.143 22)
			(0.103 28, 0.574 12, 0.141 49)	(0.110 27, 0.583 26, 0.143 10)
			(0.152 08, 0.885 38, 0.133 42)	(0.140 76, 0.906 57, 0.142 95)
$\alpha = 0.5$	$a = 5.688\,79$ Å	$a = 5.765\,10$ Å	Na: (0.238 63, 0.079 49, −0.000 38)	Na: (0.235 47, 0.077 28, −0.000 44)
$Na_{1.5}K_{0.5}ZrO_3$	$b = 9.798\,03$ Å	$b = 10.002\,12$ Å	(0.000 00, 0.098 52, 0.250 00)	(0.250 00, 0.250 00, 0.500 00)
	$c = 11.454\,24$ Å	$c = 11.069\,29$ Å	K: (0.250 00, 0.250 00, 0.500 00)	K: (0.000 00, 0.089 05, 0.250 00)
	$\beta = 100.89°$	$\beta = 100.59°$	Zr: (0.000 00, 0.432 78, 0.250 00)	Zr: (0.000 00, 0.422 98, 0.250 00)
	$V = 626.954$ Å^3	$V = 627.424$ Å^3	(0.000 00, 0.765 41, 0.250 00)	(0.000 00, 0.754 86, 0.250 00)
			O: (0.151 80, 0.283 98, 0.148 78)	O: (0.159 28, 0.286 69, 0.142 63)
			(0.081 79, 0.596 11, 0.145 83)	(0.069 45, 0.589 81, 0.140 95)
			(0.140 51, 0.919 48, 0.147 81)	(0.156 11, 0.894 16, 0.136 74)
$\alpha = 1.0$	$a = 5.517\,33$ Å	$a = 5.588\,16$ Å	Li: (0.250 00, 0.250 00, 0.500 00)	Li: (0.258 24, 0.085 30, −0.002 75)
$Na_{1.0}Li_{1.0}ZrO_3$	$b = 9.683\,52$ Å	$b = 9.789\,28$ Å	(0.000 00, 0.094 61, 0.250 00)	Na: (0.250 00, 0.250 00, 0.500 00)
	$c = 10.7740$ Å	$c = 10.706\,17$ Å	Na: (0.232 80, 0.077 07, −0.000 33)	(0.000 00, 0.097 19, 0.250 00)
	$\beta = 99.51°$	$\beta = 102.49°$	Zr: (0.000 00, 0.410 31, 0.250 00)	Zr: (0.000 00, 0.433 29, 0.250 00)
	$V = 567.716$ Å^3	$V = 571.802$ Å^3	(0.000 00, 0.742 48, 0.250 00)	(0.000 00, 0.765 22, 0.250 00)
			O: (0.139 01, 0.254 55, 0.140 16)	O: (0.142 42, 0.286 66, 0.137 38)
			(0.121 23, 0.577 28, 0.144 29)	(0.077 27, 0.597 47, 0.136 11)
			(0.147 49, 0.890 57, 0.133 88)	(0.135 49, 0.914 32, 0.135 54)
$\alpha = 1.0$	$a = 5.794\,93$ Å	$a = 5.689\,68$ Å	Na: (0.234 73, 0.075 76, −0.000 72)	Na: (0.250 00, 0.250 00, 0.500 00)
$Na_{1.0}K_{1.0}ZrO_3$	$b = 10.089\,89$ Å	$b = 9.929\,59$ Å	K: (0.250 00, 0.250 00, 0.500 00)	(0.000 00, 0.074 90, 0.250 00)
	$c = 11.572\,30$ Å	$c = 11.688\,74$ Å	(0.000 00, 0.112 53, 0.250 00)	K: (0.229 39, 0.075 25, −0.000 04)
	$\beta = 102.06°$	$\beta = 99.00°$	Zr: (0.000 00, 0.446 87, 0.250 00)	Zr: (0.000 00, 0.405 58, 0.250 00)
	$V = 661.699$ Å^3	$V = 652.245$ Å^3	(0.000 00, 0.778 24, 0.250 00)	(0.000 00, 0.738 48, 0.250 00)
			O: (0.158 34, 0.312 42, 0.148 21)	O: (0.150 00, 0.259 52, 0.150 65)
			(0.053 38, 0.611 20, 0.144 75)	(0.106 35, 0.575 01, 0.154 06)
			(0.147 74, 0.918 77, 0.142 49)	(0.15 803, 0.882 53, 0.148 99)
$\alpha = 1.5$	$a = 5.480\,04$ Å	$a = 5.524\,42$ Å	Li: (0.241 02, 0.080 36, 0.001 30)	Li: (0.250 83, 0.083 06, −0.000 68)
$Na_{0.5}Li_{1.5}ZrO_3$	$b = 9.474\,40$ Å	$b = 9.592\,64$ Å	(0.000 00, 0.085 79, 0.250 00)	(0.250 00, 0.250 00, 0.500 00)
	$c = 10.443\,55$ Å	$c = 10.164\,23$ Å	Na: (0.250 00, 0.250 00, 0.500 00)	Na: (0.000 00, 0.084 24, 0.250 00)
	$\beta = 101.01°$	$\beta = 100.79°$	Zr: (0.000 00, 0.426 21, 0.250 00)	Zr: (0.000 00, 0.417 82, 0.250 00)
	$V = 532.245$ Å^3	$V = 529.111$ Å^3	(0.000 00, 0.758 95, 0.250 00)	(0.000 00, 0.750 73, 0.250 00)
			O: (0.139 99, 0.270 23, 0.136 93)	O: (0.143 60, 0.268 73, 0.131 59)
			(0.097 03, 0.591 05, 0.134 82)	(0.093 11, 0.584 29, 0.131 74)
			(0.130 93, 0.920 84, 0.136 42)	(0.142 09, 0.900 27, 0.127 97)
$\alpha = 1.5$	$a = 5.839\,14$ Å	$a = 5.727\,82$ Å	Na: (0.250 00, 0.250 00, 0.500 00)	Na: (0.000 00, 0.083 56, 0.250 00)
$Na_{0.5}K_{1.5}ZrO_3$	$b = 10.116\,50$ Å	$b = 9.917\,88$ Å	K: (0.222 94, 0.073 71, −0.000 91)	K: (0.250 00, 0.250 00, 0.500 00)
	$c = 11.704\,95$ Å	$c = 11.992\,75$ Å	(0.000 00, 0.069 84, 0.250 00)	(0.230 79, 0.077 02, −0.000 37)
	$\beta = 99.037°$	$\beta = 99.157°$	Zr: (0.000 00, 0.402 75, 0.250 00)	Zr: (0.000 00, 0.416 15, 0.250 00)
	$V = 682.848$ Å^3	$V = 672.607$ Å^3	(0.000 00, 0.735 84, 0.250 00)	(0.000 00, 0.748 70, 0.250 00)
			O: (0.163 19, 0.267 78, 0.149 11)	O: (0.152 05, 0.267 00, 0.154 25)
			(0.079 22, 0.572 06, 0.150 52)	(0.098 18, 0.583 01, 0.153 92)
			(0.169 16, 0.870 06, 0.146 49)	(0.152 43, 0.899 60, 0.157 10)

[a]From Refs. [11,56].

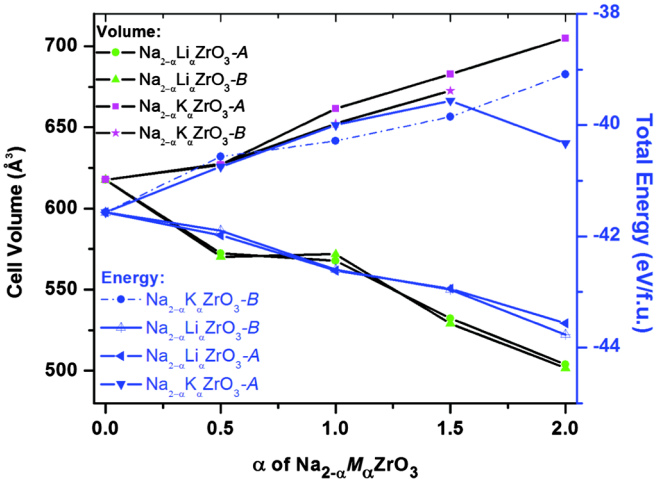

FIG. 2. The calculated cell volumes and total energies of the substituted systems with increasing concentration of the substituting elements.

From Fig. 1, it can be seen that in Na_2ZrO_3 each Zr atom is coordinated with six O's and each O coordinated with two Zr's. Along the c axis, the connected $[ZrO_3]$ groups form planar layers separated by Na layers containing two types of Na [Na(1) and Na(2)]. In the $[ZrO_3]$ layer, Zr is in the middle, the bonded O located on both sides of Zr, with one type of Na [Na(3)] atoms also located on the Zr plane as shown in Fig. 1. The relationships of the concentration of M (α) versus the calculated cell volumes and energies are shown in Fig. 2 and summarized in Tables I and II. As one can see from Fig. 2, overall, after Li substitution, the cell volumes of $Na_{2-\alpha}Li_\alpha ZrO_3$ are compressed with increasing α, while with K substitution, the cell volumes of $Na_{2-\alpha}K_\alpha ZrO_3$ are expanded with increasing α. The calculated energies of these systems have an opposite trend: the energy of $Na_{2-\alpha}Li_\alpha ZrO_3$ is decreased with increasing α, while the energy of $Na_{2-\alpha}K_\alpha ZrO_3$ is increased. In other words, when doping Li into Na_2ZrO_3, the doped $Na_{2-\alpha}Li_\alpha ZrO_3$ is stabilized in comparison with Na_2ZrO_3, while when doping K into Na_2ZrO_3, the doped $Na_{2-\alpha}K_\alpha ZrO_3$ is destabilized. Clearly, there are some differences between the $Na_{2-\alpha}M_\alpha ZrO_3$-$A$ phase and the $Na_{2-\alpha}M_\alpha ZrO_3$-$B$ phase. These results indicate that the structure of the doped system depends not only on the concentration α but also on the doping sites. Compared to M-doped Li_2ZrO_3 mixtures, Li$M$$ZrO_3$ [40], the $Na_{1.0}Li_{1.0}ZrO_3$ has a slightly lower binding energy than $LiNaZrO_3$, which means $Na_{1.0}Li_{1.0}ZrO_3$ is slightly more stable in the structure of Na_2ZrO_3 ($C12/c1$) than in the structure of Li_2ZrO_3 ($C2/c$). Obviously, such a structure difference will not only affect their electronic structural properties, but also their CO_2 capture performances.

B. Electronic structural properties

The calculated band structures of $Na_{2-\alpha}Li_\alpha ZrO_3$ and $Na_{2-\alpha}K_\alpha ZrO_3$ with different Na:Li and Na:K ratios are shown in Fig. 3 and Figs. S1 and S2 in the Supplemental

TABLE II. The calculated band gaps and valance bandwidths of $Na_{2-\alpha}M_\alpha ZrO_3$ (M = Li,K), and their corresponding DFT total energy (E_{DFT}), the zero-point energies (E_{ZP}), and the entropies (S) at T = 298 K from phonon calculations.

Crystal	VB_2 width (eV)	Gap between VB_2 and VB_3 (eV)[b]	VB_3 width (eV)	Gap between VB_3 and VB_1 (eV)	VB_1 width (eV)	Band gap (eV)	E_{DFT} (eV/f.u.)	E_{ZP} (kJ/mol)	Entropy (J/mol K)
Na_2ZrO_3[a]	0.943	11.837			3.259	4.339 (indirect) 4.83 (expt.)[e]	−41.5692	34.49	119.32
$Na_{1.5}Li_{0.5}ZrO_3$-A	1.017	11.782			3.391	4.327 (indirect) 3.65 (expt.)	−41.8992	34.39	119.29
$Na_{1.5}Li_{0.5}ZrO_3$-B	1.017	11.696			3.391	4.208 (indirect)	−41.9826	34.74	119.17
$Na_{1.5}K_{0.5}ZrO_3$-A	0.913	4.399	0.166	7.304	3.321	4.323 (direct) 4.10, 4.70 (expt.)	−40.7478	33.64	168.77
$Na_{1.5}K_{0.5}ZrO_3$-B	0.912	4.149	0.249	7.466	3.420	4.217 (indirect)	−40.5653	33.53	159.81
$Na_{1.0}Li_{1.0}ZrO_3$-A	1.027	11.724			3.423	4.175 (indirect) 3.70 (expt.)	−42.5966	34.89	117.92
$Na_{1.0}Li_{1.0}ZrO_3$-B	1.115	11.666			3.517	4.277 (indirect)	−42.5175	35.60	118.92
$Na_{1.0}K_{1.0}ZrO_3$-A	0.838	3.773	0.839	7.379	3.354	4.189 (indirect) 3.95, 4.82 (expt.)	−39.9995	33.43	155.57
$Na_{1.0}K_{1.0}ZrO_3$-B	1.030	3.518	0.858	7.552	3.175	4.249 (indirect)	−40.2861	33.46	166.22
$Na_{0.5}Li_{1.5}ZrO_3$-A	1.126	11.607			3.552	4.164 (direct) 4.10 (expt.)	−42.9598	35.10	123.38
$Na_{0.5}Li_{1.5}ZrO_3$-B	1.142	11.599			3.603	4.152 (indirect)	−42.9386	33.14	117.39
$Na_{0.5}K_{1.5}ZrO_3$-A	0.919	3.343	1.170	7.606	3.175	4.211 (indirect) 4.92 (expt.)	−39.5602	33.31	151.06
$Na_{0.5}K_{1.5}ZrO_3$-B	1.091	2.855	1.175	7.893	3.190	4.147 (direct)	−39.8518	33.39	169.16
Li_2ZrO_3[c]	1.010	11.695			3.730	3.898 (indirect)	−43.7685−43.5635[d]	36.11	101.88
K_2ZrO_3[c]	0.973	2.839	0.487	8.921	2.757	3.641 (direct)	−40.3284−39.0854[d]	28.49	168.65

[a]Taken from Ref. [11].
[b]For those systems without VB_3, this gap refers to the gap between VB_2 and VB_1.
[c]Taken from Ref. [10].
[d]Calculated within the structure of Na_2ZrO_3.
[e]Experimental measured value. Two values means two potassium-substituted samples have two absorption features.

Material [55], respectively. Table II summarizes their bandwidths and band gaps. The experimentally measured band gaps of $Na_{2-\alpha}Li_{\alpha}ZrO_3$ and $Na_{2-\alpha}K_{\alpha}ZrO_3$ with $\alpha = 0.5$, 1.0, 1.5 are also listed in Table II. The diffuse reflectance data for Li- and K-substituted Na_2ZrO_3 are shown in Figs. S3 and S4 of the Supplemental Material [55]. For $Na_{1.5}K_{0.5}ZrO_3$ and $Na_{1.0}K_{1.0}ZrO_3$, we make two different samples to measure their band gaps. As listed in Table II, their results show two absorption features with different values of band gaps (4.1,4.7 eV and 3.95,4.82 eV), which could be due to two phases or two different transitions in the same phase.

From these figures, one can see that the band structures of $Na_{2-\alpha}Li_{\alpha}ZrO_3$ for different doping levels ($\alpha = 0.5,1.0,1.5$) and configurations (case *A* and *B*) have some similarities. They have two valence bands (VBs) and their shapes look similar to each other. Their second VBs (VB_2) are located below -15 eV with narrow bandwidth while their first VBs (VB_1) are just below the Fermi energy with very wide width. All of the $Na_{2-\alpha}Li_{\alpha}ZrO_3$ compounds have large gaps (>11.5 eV) between VB_1 and VB_2. Except for $Na_{0.5}Li_{1.5}ZrO_3$-*A*, which has a direct band gap, all others have indirect band gaps located between the Γ and *M* high-symmetry points. Figure 3 demonstrates that increasing the Li doping level results in a slight decrease of the band-gap energy. At the same Li doping level, the band gap has a small difference of about 0.1 eV between case *A* and case *B*. Comparing $Na_{2-\alpha}Li_{\alpha}ZrO_3$ with corresponding pure Na_2ZrO_3 and Li_2ZrO_3, when doping Li into Na_2ZrO_3, the band gaps of the obtained $Na_{2-\alpha}Li_{\alpha}ZrO_3$ are bigger than pure Na_2ZrO_3 (3.295 eV) [11] but smaller than that of Li_2ZrO_3 (3.73 eV) [10].

Similar results also can be found in the band structures of $Na_{2-\alpha}K_{\alpha}ZrO_3$ as shown in Fig. 3 and Figs. S1 and S2 of the Supplemental Material [55]. Compared to $Na_{2-\alpha}Li_{\alpha}ZrO_3$, one can see that in the case of $Na_{2-\alpha}K_{\alpha}ZrO_3$, between VB_1 and VB_2, there is another VB (VB_3) which is contributed by the doped-K element. As summarized in Table II, for each $Na_{2-\alpha}K_{\alpha}ZrO_3$ configuration, the gap between VB_2 and VB_3 is much smaller than that between VB_1 and VB_3. Obviously, with increasing K-doping levels, the widths of VB_3 are increased. In this case, only $Na_{1.5}K_{0.5}ZrO_3$-*A* and $Na_{0.5}K_{1.5}ZrO_3$-*B* have direct band gaps while other configurations have indirect band gaps located between the Γ and *M* high-symmetry points. As summarized in Table II, the bandwidths of the first and second VBs for $Na_{2-\alpha}K_{\alpha}ZrO_3$ with different K-doping levels are close to each other. Compared to pure Na_2ZrO_3 and K_2ZrO_3, when

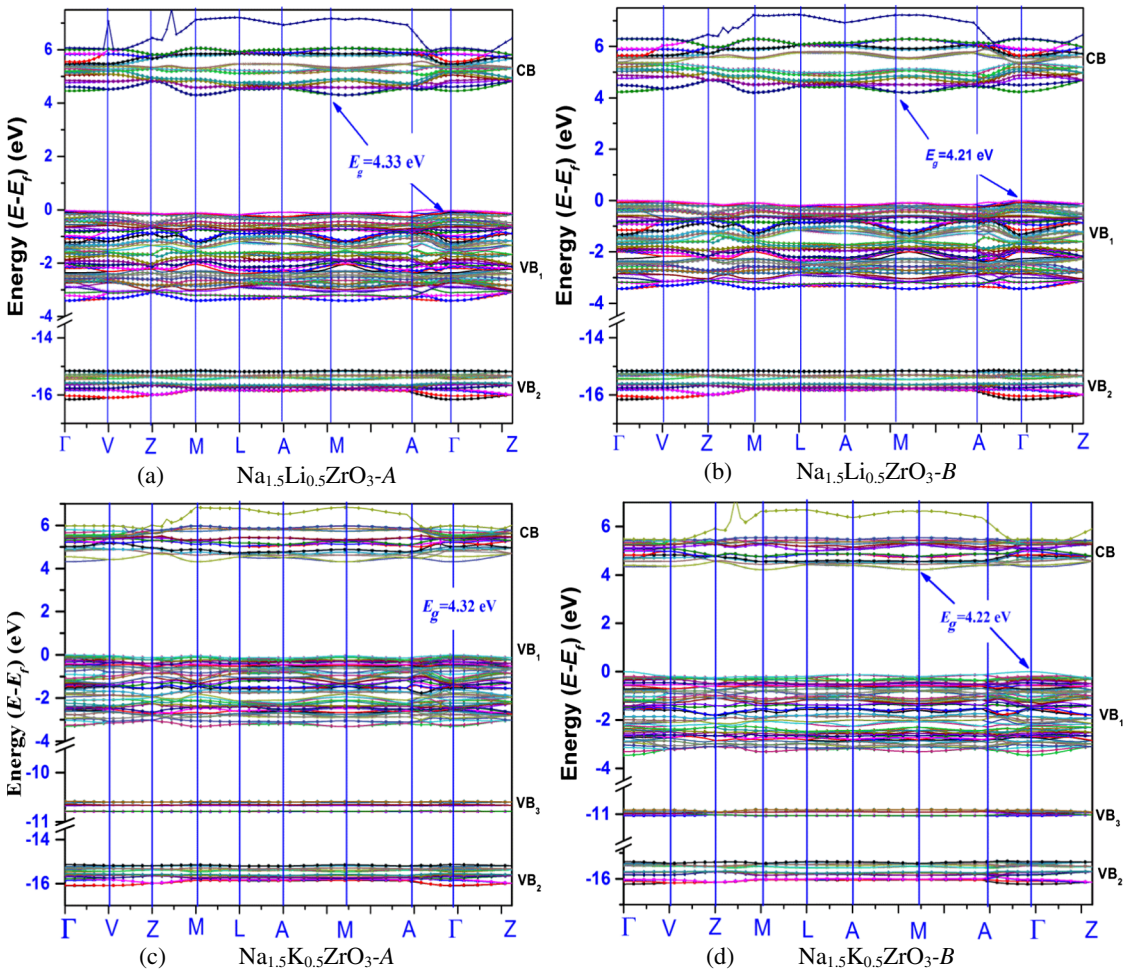

FIG. 3. The calculated band structures of $Na_{1.5}M_{0.5}ZrO_3$ (M = Li,K).

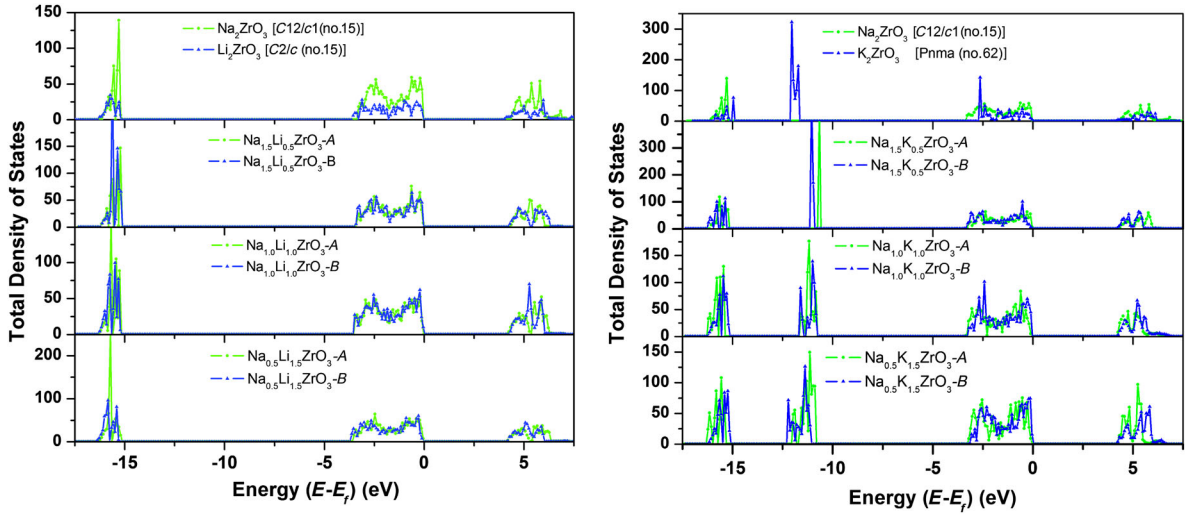

FIG. 4. The calculated total density of states of $Na_{2-\alpha}M_{\alpha}ZrO_3$ ($\alpha = 0.5,1.0,1.5$). For comparison, the calculated total density of states of M_2ZrO_3 (M = Li,Na,K) is also shown in the figure. (a) $Na_{2-\alpha}Li_{\alpha}ZrO_3$. (b) $Na_{2-\alpha}K_{\alpha}ZrO_3$.

doping K into Na_2ZrO_3, the band gaps of the obtained $Na_{2-\alpha}K_{\alpha}ZrO_3$ are similar to pure Na_2ZrO_3 (3.295 eV), but larger than that of K_2ZrO_3 (2.76 eV) [11]. Part of the reason for this is that their crystal structures are quite different. Different from pure Li_2ZrO_3, pure K_2ZrO_3 has an orthorhombic symmetry while $Na_{2-\alpha}K_{\alpha}ZrO_3$ and Na_2ZrO_3 have monoclinic symmetries.

Figure 4 shows the calculated total density of states (TDOS) of $Na_{2-\alpha}M_{\alpha}ZrO_3$. As an example, Fig. 5 gives the corresponding partial density of states (PDOS) of $Na_{1.5}M_{0.5}ZrO_3$. Other PDOS of $Na_{2-\alpha}M_{\alpha}ZrO_3$ with M-doping levels of $\alpha = 1.0$ and 1.5 are shown in Figs. S5 and S6 of the Supplemental Material [55], respectively. It can be seen from Fig. 4(a), after doping with Li into Na_2ZrO_3, the TDOS of $Na_{2-\alpha}Li_{\alpha}ZrO_3$-$A$ and $Na_{2-\alpha}Li_{\alpha}ZrO_3$-$B$ are similar to each other. With increasing Li-doping level, the TDOS as well as the PDOS of $Na_{2-\alpha}Li_{\alpha}ZrO_3$ do not have significant changes. In contrast, when doping the same level of K into Na_2ZrO_3, the TDOS and PDOS of $Na_{2-\alpha}K_{\alpha}ZrO_3$-$A$ and $Na_{2-\alpha}K_{\alpha}ZrO_3$-$B$ have significant differences as shown in Figs. 4(b), 5(b), and Figs. S5 and S6 in the Supplemental Material [55], which means that the doping sites do play a significant role in their electronic properties. With increasing K-doping level, the VB_3, formed solely by K p orbitals, is broader, shifted to a higher energy range, and split into more than one subband, as shown in Figs. 3–5 and Figs. S1, S2, S5, and S6 [55].

C. Dynamical phonon properties

As described in Sec. IV A, there are eight unit formulas ($Z = 8$) in the Na_2ZrO_3 unit cell. However, its primitive

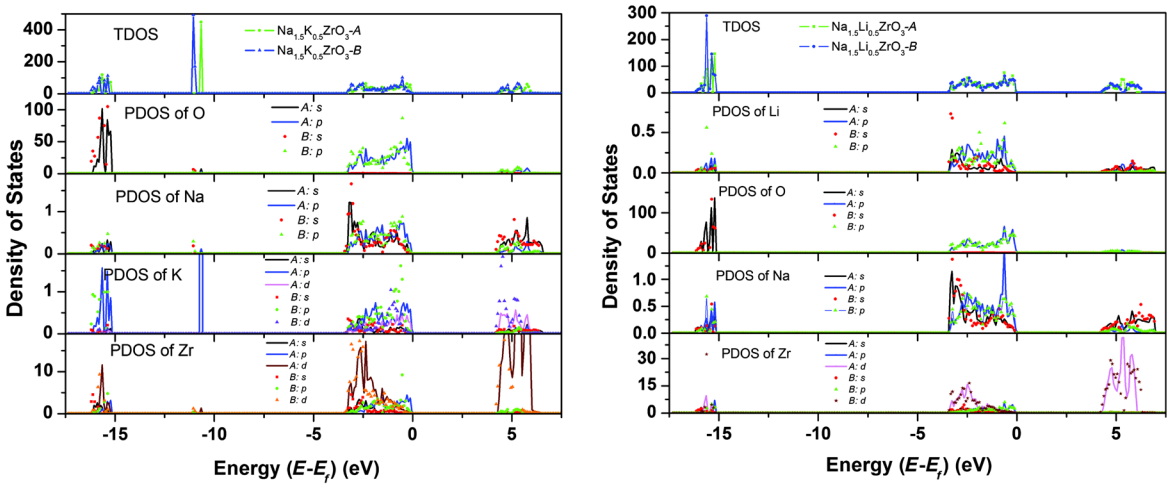

FIG. 5. The calculated partial density of states of $Na_{1.5}M_{0.5}ZrO_3$.

cell only contains four formula units. Therefore, there are 72 phonon modes in all $Na_{2-\alpha}M_{\alpha}ZrO_3$ ($M = \mathrm{Li,K}$) because the doped systems have the same symmetry as Na_2ZrO_3, with corresponding point group C_{2h}, which has the following representations:

$$\Gamma_m^b = 15A_g(R) \oplus 18B_g(R) \oplus 18A_u(I) \oplus 21B_u(I). \quad (10)$$

Obviously, all of the vibrational modes are nondegenerate (A_u, A_g, B_u, and B_g) because their crystal point groups are quite low with C_{2h}. Among these vibrational modes, 33 are only Raman active, while 39 are only infrared active.

As an example, the calculated phonon dispersions of $Na_{1.5}M_{0.5}ZrO_3$ are shown in Fig. 6. Other calculated phonon dispersions of $Na_{1.0}M_{1.0}ZrO_3$ and $Na_{0.5}M_{1.5}ZrO_3$ are shown in Figs. S7 and S8 of the Supplemental Material [55], respectively. Obviously, there are two soft modes in $Na_{1.5}Li_{0.5}ZrO_3$-A, one soft mode in $Na_{1.0}Li_{1.0}ZrO_3$-A, and four soft modes in $Na_{0.5}Li_{1.5}ZrO_3$-B, which indicate these structures are not stable compared to other configurations at different Li-doping levels. Such results are consistent with the calculated DFT total energies listed in Table II. In contrast, for K-doped Na_2ZrO_3 systems, only $Na_{1.5}K_{0.5}ZrO_3$-B has a few soft modes. These results indicate that the Na_2ZrO_3 is more stable when doped with K than with Li. It should be pointed out that although these doped systems with soft modes are less stable (compared to corresponding ones without soft modes and will not be used for the following CO_2 capture analysis), further understanding what causes these soft modes is an interesting topic which may lead to other useful applications.

The calculated total phonon density of states (TPDOS) of $Na_{2-\alpha}Li_{\alpha}ZrO_3$ and $Na_{2-\alpha}K_{\alpha}ZrO_3$ are shown in Fig. 7. It can be seen that there are some differences between TPDOS of $Na_{2-\alpha}M_{\alpha}ZrO_3$-$A$ and $Na_{2-\alpha}M_{\alpha}ZrO_3 - B$. With increasing Li-doping level, the TPDOS spans to a

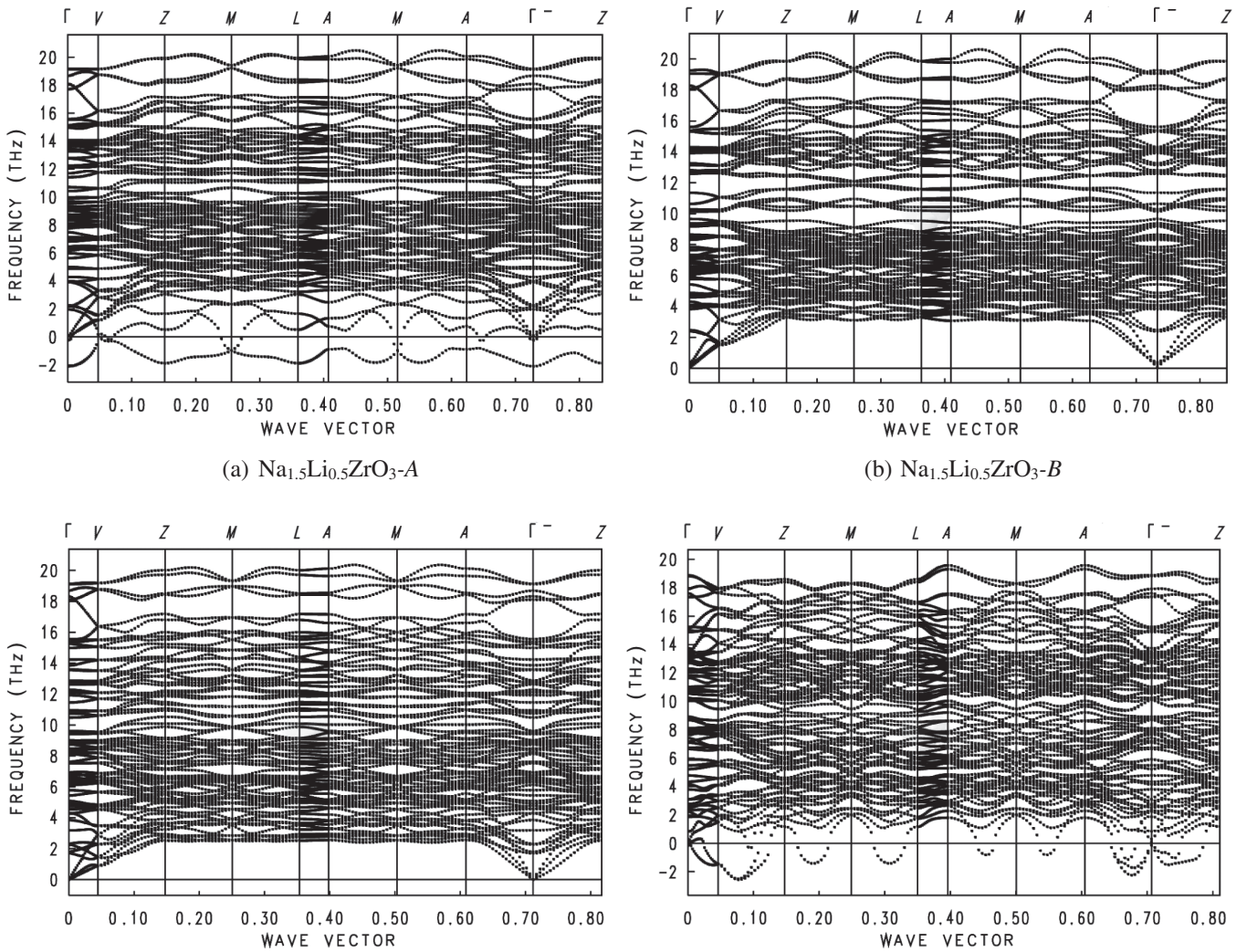

(a) $Na_{1.5}Li_{0.5}ZrO_3$-A (b) $Na_{1.5}Li_{0.5}ZrO_3$-B

(c) $Na_{1.5}K_{0.5}ZrO_3$-A (d) $Na_{1.5}K_{0.5}ZrO_3$-B

FIG. 6. Phonon dispersion curves of $Na_{1.5}M_{0.5}ZrO_3$ ($M = \mathrm{Li,K}$).

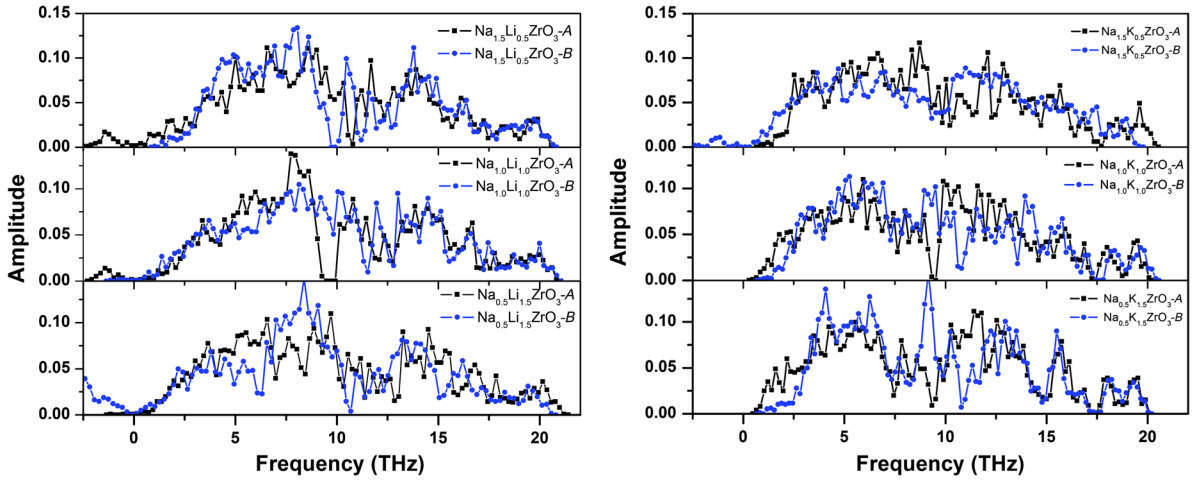

FIG. 7. Total phonon density of states. (a) $Na_{2-\alpha}Li_{\alpha}ZrO_3$. (b) $Na_{2-\alpha}K_{\alpha}ZrO_3$, $\alpha = 0.5,1.0,1.5$.

higher frequency range while, with increasing K-doping level, the TPDOS shrinks to lower frequency. The reason is that the Li is lighter than Na while K is heavier than Na.

Based on the calculated phonon dispersion frequencies and density of states, the phonon free energy [F^{ph} (T)] and entropy [S^{ph} (T)] of doped systems $Na_{2-\alpha}M_{\alpha}ZrO_3$ versus temperatures are evaluated and shown in Figs. 8 and 9, respectively. Obviously, the zero-point energy (E_{ZP}) can be obtained from Fig. 8 by setting $T = 0$ K. In Table II, we list the calculated zero-point energies and the room-temperature entropies of these doped systems $Na_{2-\alpha}M_{\alpha}ZrO_3$. Overall, the entropies of $Na_{2-\alpha}K_{\alpha}ZrO_3$ are larger than corresponding $Na_{2-\alpha}Li_{\alpha}ZrO_3$. It can be seen from Figs. 8 and 9, that with increasing the Li- or K-doping level, although there are some differences, the $F^{\mathrm{ph}}(T)$ and $S^{\mathrm{ph}}(T)$ do not change much. Therefore, according to Eqs. (2) and (3), the E^{DFT} plays an important role for evaluating the thermodynamic properties of the CO_2 capture reactions by these doped solids. In the following thermodynamic analysis, we only use those systems without soft modes and with lower E^{DFT}.

D. Capabilities of CO_2 capture

Experimental investigations showed that the alkali-metal zirconates are potential solid sorbents for CO_2 capture because of their large CO_2 sorption capacity, infinite CO_2-N_2 or CO_2-H_2 selectivity, good reversibility, and high operating temperature [4,18–33]. From Eq. (1), when $P_{CO_2} = P_0 = 1$ bar, the $\Delta\mu(T)$ is identical to the standard Gibbs free-energy change $\Delta G(T)$. According to Eqs. (1), (2), and (3), the calculated thermodynamic properties [$\Delta H(T)$, $\Delta G(T)$, $\Delta S(T)$] of the capture reactions [given above Eq. (1)] versus the temperatures are plotted in Fig. 10 and also summarized in Table III.

One can see from Figs. 10(a) and 10(b), for all doped systems reacting with CO_2, the heat of reaction $\Delta H(T)$ and the entropy change $\Delta S(T)$ are decreased with increasing temperatures. Such results indicate that the entropy gain

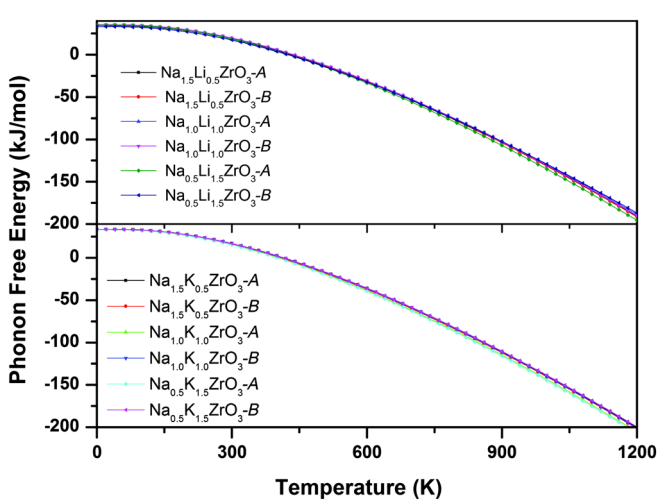

FIG. 8. The calculated phonon free energies versus temperatures of $Na_{2-\alpha}M_{\alpha}ZrO_3$, $M = \mathrm{Li,K}$, $\alpha = 0.5,1.0,1.5$.

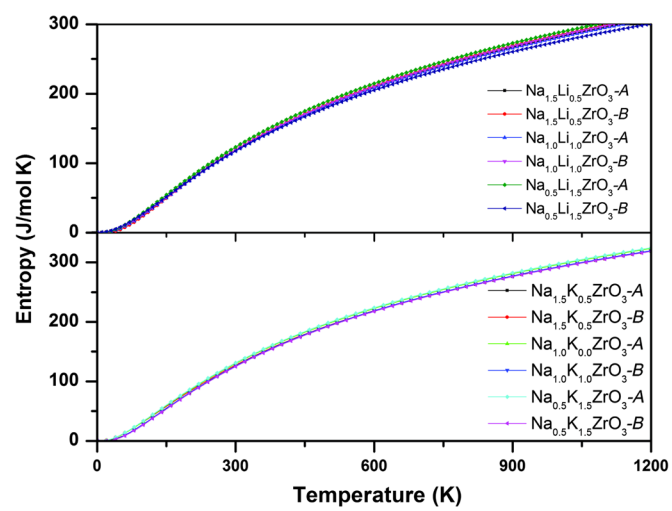

FIG. 9. The calculated entropies versus temperatures of $Na_{2-\alpha}M_{\alpha}ZrO_3$, $M = \mathrm{Li,K}$, $\alpha = 0.5,1.0,1.5$.

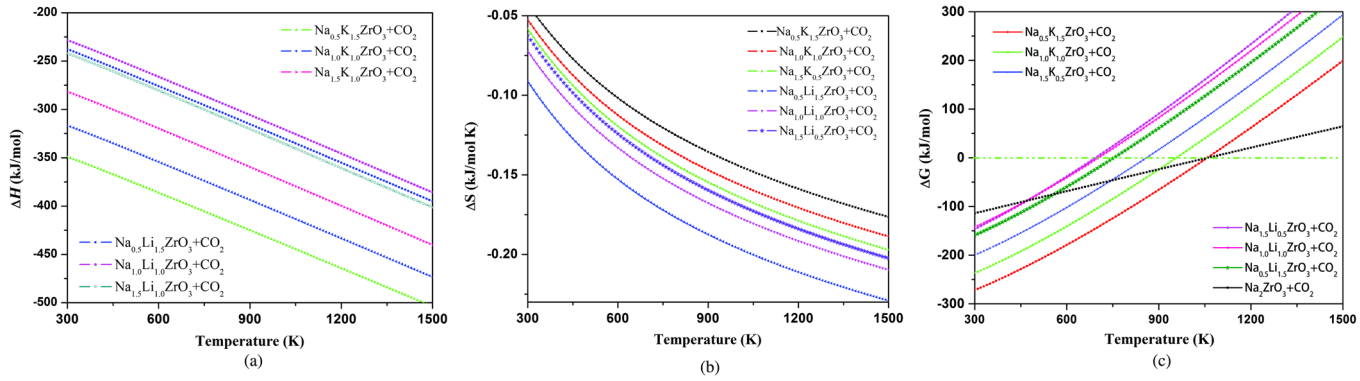

FIG. 10. The calculated thermodynamic properties of the reactions of $Na_{2-\alpha}M_{\alpha}ZrO_3$ (M = Li,K, α = 0.5,1.0,1.5) capturing CO_2. (a) The heat of reaction versus temperature. (b) The entropy change of the reaction versus temperature. (c) Gibbs free-energy change versus temperature.

associated with releasing CO_2 from the corresponding carbonates gets larger as one raises the temperature. However, the Gibbs free-energy changes of the CO_2 capture reactions by these mixed sorbents increase with the increasing temperatures and reach zero at a certain turnover temperature (T_t) for different mixtures, as shown in Fig. 10(c). Above T_t, the doped material will not absorb CO_2 anymore and the capture reaction starts to reverse to release CO_2.

According to Eq. (1), for the reactions of $Na_{2-\alpha}M_{\alpha}ZrO_3$ capturing CO_2, we can explore the relationship among the chemical-potential change [$\Delta\mu(T,P)$], the temperature (T), and the CO_2 pressure (P_{CO_2}). In Fig. 11, we show this kind of relationship (van 't Hoff plots) for the capture reactions. For comparison, the results of pure M_2ZrO_3 (M = Li,Na, K) [10,11] are also plotted in the same figure. The line in Fig. 11 indicates that for each CO_2 capture reaction, the $\Delta\mu(T,P) \to 0$. Around the line is a good region for the absorption and desorption because the energy costs of performing absorption and desorption are low. Above the line, the solid $Na_{2-\alpha}M_{\alpha}ZrO_3$ is favored to absorb CO_2 and to form carbonates M_2CO_3 and ZrO_2, while below the line the carbonates are favored to release CO_2 and regenerate the initial solids.

As described above and shown in Fig. 11, all of the absorption reactions have the potential to be thermodynamically favorable over quite a wide range of temperatures (<1000 K) and P_{CO_2}, which means in this temperature range the CO_2 absorption is thermodynamically favored in $Na_{2-\alpha}M_{\alpha}ZrO_3$. But as a CO_2 solid sorbent, the sorbent should not only easily absorb CO_2 at the first half-cycle but also should be easily regenerated from products (M_2CO_3 and ZrO_2, for example) to release the CO_2 at the second half-cycle. The operating conditions of absorption or desorption depend on the pre- and postcombustion technologies. Under precombustion conditions, after the water-gas shift reaction, the gas stream mainly contains CO_2, H_2O, and H_2. The partial CO_2 pressure is around 20–25 bar and the

TABLE III. The weight percentage of CO_2 capture, the ratios of $Na_2O:M_2O:ZrO_2$ (M = Li,K), the calculated energy change ΔE^{DFT}, the zero-point energy changes ΔE^{ZP}, and the thermodynamic properties (ΔH, ΔG) of the CO_2 capture reactions (units are kJ/mol). The turnover temperatures (T_1 and T_2) of the reactions of CO_2 capture by solids under the conditions of precombustion (P_{CO_2} = 20 bar) and postcombustion (P_{CO_2} = 0.1 bar) are also listed.

Reaction	Absorbing CO_2 wt %	$Na_2O:M_2O:ZrO_2$ ratio	ΔE^{DFT}	ΔE^{ZP}	ΔH (T=300 K)	ΔG (T=300 K)	Turnover T (K) T_1	Turnover T (K) T_2
$Na_2ZrO_3 + CO_2 \leftrightarrow Na_2CO_3 + ZrO_2$[a]	23.76	1:0:1	−140.862	2.236	−158.327	−114.121	1275	925
$Na_{1.5}Li_{0.5}ZrO_3$-$B + CO_2 \leftrightarrow (3/4)Na_2CO_3 + (1/4)Li_2CO_3 + ZrO_2$	24.83	3/4:1/4:1	−170.881	4.667	−242.090	−159.144	805	715
$Na_{1.0}Li_{1.0}ZrO_3$-$B + CO_2 \leftrightarrow (1/2)Na_2CO_3 + (1/2)Li_2CO_3 + ZrO_2$	26.01	1/2:1/2:1	−157.839	6.480	−228.381	−142.555	745	675
$Na_{0.5}Li_{1.5}ZrO_3$-$A + CO_2 \leftrightarrow (1/4)Na_2CO_3 + (3/4)Li_2CO_3 + ZrO_2$	27.31	1/4:3/4:1	−169.827	9.652	−237.765	−146.230	735	665
$Na_{1.5}K_{0.5}ZrO_3$-$A + CO_2 \leftrightarrow (3/4)Na_2CO_3 + (1/4)K_2CO_3 + ZrO_2$	22.77	3/4:1/4:1	−210.081	2.486	−281.253	−199.996	915	825
$Na_{1.0}K_{1.0}ZrO_3$-$B + CO_2 \leftrightarrow (1/2)Na_2CO_3 + (1/2)K_2CO_3 + ZrO_2$	21.86	1/2:1/2:1	−245.436	2.058	−316.736	−236.789	1015	915
$Na_{0.5}K_{1.5}ZrO_3$-$B + CO_2 \leftrightarrow (1/4)Na_2CO_3 + (3/4)K_2CO_3 + ZrO_2$	21.02	1/4:3/4:1	−278.147	1.519	−349.077	−272.038	1125	1015
$Li_2ZrO_3 + CO_2 \leftrightarrow Li_2CO_3 + ZrO_2$[b]	28.75	0:1:1	−146.648	11.311	−158.562	−103.845	1000	780
$K_2ZrO_3 + CO_2 \leftrightarrow K_2CO_3 + ZrO_2$[a]	20.24	0:1:1	−223.158	5.813	−238.490	−187.884	HT[c]	1285

[a]From Ref. [11].
[b]From Ref. [10].
[c]HT means the temperature is higher than 1500 K.

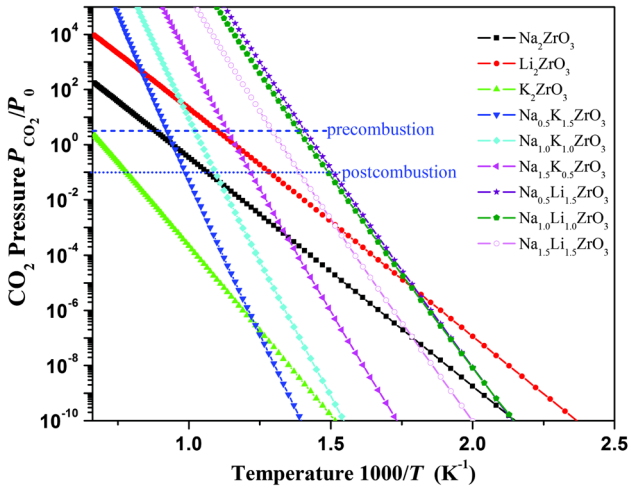

FIG. 11. Contour plot of calculated chemical-potential changes versus CO_2 pressures and temperatures of the reactions for $Na_{2-\alpha}M_\alpha ZrO_3$ ($M = \mathrm{Li,K}$, $\alpha = 0.5,1.0,1.5$) capture of CO_2. The typical CO_2 pressures for pre- and postcombustions are given in blue lines. The y axis is plotted in logarithm scale. Only the $\Delta\mu = 0$ curve is shown explicitly. For each reaction, above its $\Delta\mu = 0$ curve, $\Delta\mu < 0$, which means $Na_{2-\alpha}M_\alpha ZrO_3$ absorbs CO_2 and the reaction goes forward, whereas below the $\Delta\mu = 0$ curve, $\Delta\mu > 0$, which means the CO_2 starts to release and the reaction goes backward to regenerate the sorbents.

temperature is around 300–350 °C. For precombustion, the programmatic goal of the Department of Energy (DOE) is to capture at least 90% CO_2 with cost in electricity no more than 10% [62,63]. To minimize energy consumption, the ideal sorbents should work within these pressure and temperature ranges to separate CO_2 from H_2. The turnover temperature at these pressures, denoted T_1, is listed in Table III, and is the temperature above which the $Na_{2-\alpha}M_\alpha ZrO_3$ cannot absorb CO_2 anymore and will start to release CO_2. This result indicates during the first half cycle when CO_2 is captured, the operating temperature should be lower than T_1, whereas the operating temperature may be higher than T_1 (depending on the desired CO_2 pressure) during the second half-cycle when sorbents regenerate and release CO_2. For postcombustion conditions, the gas stream mainly contains CO_2 and N_2, the partial pressure of CO_2 is around 0.1–0.2 bar, and the temperature range is quite different, but the low-temperature capture is desired. The DOE programmatic goal for postcombustion and oxycombustion CO_2 capture is to capture at least 90% CO_2 with the cost in electricity no more than 35%, whereas in the case of precombustion CO_2 capture, the goal is to capture at least 90% CO_2 with the cost in electricity no more than 10% [62,63]. The turnover temperatures (denoted as T_2) for postcombustion capture CO_2 by $Na_{2-\alpha}M_\alpha ZrO_3$ are also listed in Table III.

From Table III and Fig. 11, one can see that, compared with the desired precombustion condition (573–723 K), only $Na_{1.0}Li_{1.0}ZrO_3$ and $Na_{0.5}Li_{1.5}ZrO_3$ have their T_1 close to the high end of the precombustion condition. Therefore, when doping at least 50% Li into Na_2ZrO_3, the newly formed Li-doped Na_2ZrO_3 could be used for precombustion CO_2 capture technology. Obviously, the lower Li-doped (<50%) and all K-doped Na_2ZrO_3 are not good sorbents for capturing CO_2 in precombustion technology. However, all of the Li- and K-doped Na_2ZrO_3 materials could be used for high-temperature postcombustion CO_2 capture with T_2 in the range of 665 K–1015 K as listed in Table III.

Compared to pure Na_2ZrO_3, the Li- and K-doped mixtures have lower turnover temperatures. The amount by which T_t is shifted not only depends on the doped element, but also depends on the doping level. Obviously, as shown in Table III and Fig. 11, the Li-doped systems have a larger T_t decrease than the K-doped systems. When increasing Li-doping level α, the T_t of the corresponding mixture $Na_{2-\alpha}Li_\alpha ZrO_3$ decreases further to a low-temperature range. However, in the case of K-doped systems $Na_{2-\alpha}K_\alpha ZrO_3$, doping K into Na_2ZrO_3 initially shifts its T_t to lower temperatures but further increase in the K-doping level α causes T_t to increase. In other words, Li doping of Na_2ZrO_3 has a more beneficial influence on its CO_2 capture performance than K doping.

Figure 12 shows the CO_2 capture performances of pure Na_2ZrO_3 and one doping level $\alpha = 0.5$ $Na_{1.5}M_{0.5}ZrO_3$. The experimental results clearly show that, compared to pure Na_2ZrO_3, both $Na_{1.5}Li_{0.5}ZrO_3$ and $Na_{1.5}K_{0.5}ZrO_3$ have higher CO_2 capture capacities. Compared to $Na_{1.5}K_{0.5}ZrO_3$, the $Na_{1.5}Li_{0.5}ZrO_3$ has higher CO_2 capacity and reaches to the maximum faster and at lower temperature.

At low temperatures, the superficial CO_2 captures are not so different, although the final ones (associated with the bulk capture process) are significantly different, among the samples. While the pristine Na_2ZrO_3 captured 9.11 wt %, $Na_{1.5}Li_{0.5}ZrO_3$ and $Na_{1.5}K_{0.5}ZrO_3$ captured 18.35 and 14.54 wt %, respectively. Although the dynamic TGA experiments are qualitative results, it seems that the CO_2

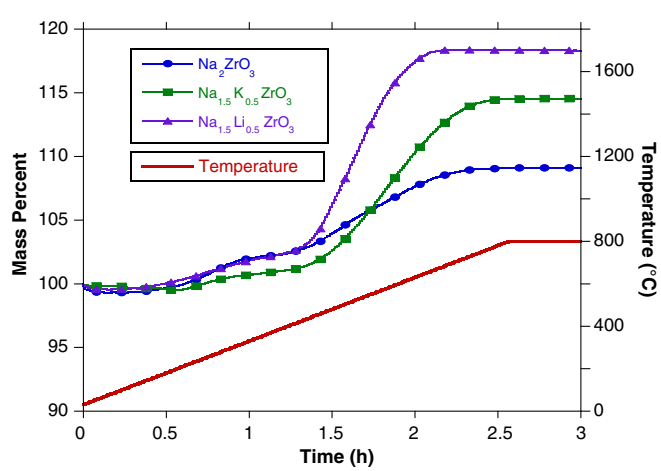

FIG. 12. TGA measurements of CO_2 capture by $Na_{1.5}M_{0.5}ZrO_3$ ($M = \mathrm{Li,K}$), compared to pure Na_2ZrO_3.

bulk capture process (400–750 °C) in $Na_{1.5}M_{0.5}ZrO_3$ samples is faster than in Na_2ZrO_3. The slopes obtained in the Na_2ZrO_3 sample (0.019 wt %/°C) is smaller than those obtained in the $Na_{1.5}Li_{0.5}ZrO_3$ (0.066 wt %/°C) and $Na_{1.5}K_{0.5}ZrO_3$ (0.041 wt %/°C) samples. All of these results are in good agreement with our calculated results as discussed above.

Apart from the theoretical data discussed and experimentally corroborated above, all of these results validate different diffusion and kinetic analyses previously reported. In a previous study [30], the experimental results clearly showed that CO_2 capture in $Na_{2-\alpha}Li_\alpha ZrO_3$ samples increased significantly, as a function of the lithium content. However, as shown in Figs. 10 and 11, the theoretical results here did not anticipate such a high difference. Thus, the explanation must be related to kinetic factors. The kinetic factors may be related to the structural variations mentioned previously and/or to eutectic phase formation $[(Na, Li)_2CO_3]$, which induces a partial fusion. In any case, the diffusion processes must be enhanced due to mixing the alkaline elements in the $Na_{2-\alpha}M_\alpha ZrO_3$ and further calculations are under way. It should be pointed it out that, in order to fully understand the kinetic mechanisms of CO_2 sorption or desorption by those thermodynamically feasible solid materials, simulations are in high demand for CO_2 reacting with a sorbent and diffusing through the formed carbonate shell as well as for the formation of products.

$Na_{2-\alpha}M_\alpha ZrO_3$ materials can be stoichiometrically regarded as a mixture of three oxides: Na_2O, M_2O, ZrO_2 in the ratio $(2-\alpha):\alpha:1$. In Table III, we list these ratios for the corresponding M-doped Na_2ZrO_3 with different doping levels. As we know, for a given CO_2 capture process, the optimal working temperature range (ΔT_O) is desired to be fixed. Meanwhile, at a given CO_2 pressure, the T_t of an individual solid capture CO_2 reaction is also fixed. However, such T_t may be outside the ΔT_O for a particular capture technology. In order to adjust T_t to fit the ΔT_O, we demonstrate that this adjustment can be achieved by mixing two different types of solids to shift T_t to the practical operating ΔT_O range [7–9]. This study further provides ways that mixing or doping more than two oxides to form new sorbents can fit the industrial needs to capture CO_2 with better performance and proper working conditions.

V. SUMMARY AND CONCLUSIONS

We investigate the electronic structural and phonon properties of $Na_{2-\alpha}M_\alpha ZrO_3$ (M = Li,K, α = 0,0.5,1.0, 1.5,2.0) by density-functional theory and first-principles determination of phonon dynamics. The thermodynamic properties of CO_2 absorption or desorption in these materials are analyzed.

With increasing doping level α, the binding energies of $Na_{2-\alpha}Li_\alpha ZrO_3$ increase while the binding energies of $Na_{2-\alpha}K_\alpha ZrO_3$ decrease, destabilizing the structure. The $Na_{2-\alpha}Li_\alpha ZrO_3$ for different doping levels (α = 0.5,1.0,1.5) and configurations (case A and B) have two VBs and their shapes look similar to each other. Except for $Na_{0.5}Li_{1.5}ZrO_3$-A which has a direct band gap, all others have indirect band gaps located between the Γ and M high-symmetry points. However, in the case of $Na_{2-\alpha}K_\alpha ZrO_3$, between VB_1 and VB_2, there is another VB_3, which is contributed by the doped-K element and its width is increased with increasing K-doping level. Compared to pure M_2ZrO_3 (M = Li,Na,K), due to their different crystal structures, when doping Li into Na_2ZrO_3, the band gaps of the obtained $Na_{2-\alpha}K_\alpha ZrO_3$ are larger than those of pure Na_2ZrO_3 but smaller than those of Li_2ZrO_3. When doping K into Na_2ZrO_3, the band gaps of the obtained $Na_{2-\alpha}K_\alpha ZrO_3$ are similar to those of pure Na_2ZrO_3 but larger than those of K_2ZrO_3. The calculated density of states showed that, at the same doping level, the doping sites play significant roles in the electronic properties.

As in Na_2ZrO_3, $Na_{2-\alpha}M_\alpha ZrO_3$ possesses 72 phonon modes. Among them, 33 modes are Raman active and 39 modes are infrared active only. Calculated imaginary frequencies found in several doped configurations indicate that the structures are not stable compared to other configurations with different doping levels. Based on the calculated phonon frequencies and density of states, the obtained phonon free energies and entropies of $Na_{2-\alpha}M_\alpha ZrO_3$ (with different doping levels α and different doping sites) do not have large differences with increasing temperature. Hence, the calculated E^{DFT} of each doped system plays an important role for evaluating the thermodynamic properties of CO_2 capture reactions.

From the calculated relationships among the chemical-potential change, the CO_2 pressure and the temperature for CO_2 capture reactions by $Na_{2-\alpha}M_\alpha ZrO_3$, and from TGA experimental measurements, the Li- and K-doped mixtures ($Na_{2-\alpha}M_\alpha ZrO_3$) have lower turnover temperatures and higher CO_2 capacities than the pure Na_2ZrO_3. The calculated results show that the shift in T_t depends not only on the doping element, but also depends on the doping level. The Li-doped systems have larger T_t decreases than the K-doped systems. When increasing the Li-doping level α, the T_t of the corresponding mixture $Na_{2-\alpha}Li_\alpha ZrO_3$ decreases further to a low-temperature range. However, in the case of K-doped systems $Na_{2-\alpha}K_\alpha ZrO_3$, although initial doping of K into Na_2ZrO_3 can shift its T_t to a lower temperature range, further increasing the K-doping level α results in an increase in T_t. Therefore, compared to K-doping, lithium inclusion into a Na_2ZrO_3 structure has a larger influence on the CO_2 capture performance.

All of these results may be of interest in the development of specific CO_2 capture applications. As is shown, the $Na_{2-\alpha}Li_\alpha ZrO_3$ and $Na_{2-\alpha}K_\alpha ZrO_3$ compositions can produce modifications in the CO_2 capture temperatures, which may be used in the design of a specific composition depending on the temperature range that industry requires. Our work shows that the capture of CO_2 in zirconate

materials is not simply a matter of a substitutional element, but also relies on the doping level. This insight needs to be considered during future sorbent development. We also demonstrate that computational methods can be used to accurately predict aspects of CO_2 capture and such methods the potential to drive future work by identifying the most promising candidate materials.

[1] D. Aaron and C. Tsouris, Separation of CO_2 from flue gas: A review, Sep. Sci. Technol. **40**, 321 (2005).

[2] C. M. White, B. R. Strazisar, E. J. Granite, J. S. Hoffman, and H. W. Pennline, Separation and capture of CO_2 from large stationary sources and sequestration in geological formations—coalbeds and deep saline aquifers, J. Air Waste Manag. Assoc. **53**, 645 (2003).

[3] R. S. Haszeldine, Carbon capture and storage: How green can black be?, Science **325**, 1647 (2009).

[4] H. Pfeiffer and P. Bosch, Thermal stability and high-temperature carbon dioxide sorption on hexa-lithium zirconate ($Li_6Zr_2O_7$), Chem. Mater. **17**, 1704 (2005).

[5] E. Ochoa-Fernandez, H. K. Rusten, H. A. Jakobsen, M. Ronning, A. Holmen, and D. Chen, Sorption enhanced hydrogen production by steam methane reforming using Li_2ZrO_3 as sorbent: Sorption kinetics and reactor simulation, Catal. Today **106**, 41 (2005).

[6] B. Y. Li, Y. Duan, D. Luebke, and B. Morreale, Advances in CO_2 capture technology: A patent review, Applied Energy **102**, 1439 (2013).

[7] Y. Duan, Structural and electronic properties of Li_8ZrO_6 and its CO_2 capture capabilities: An *ab initio* thermodynamic approach, Phys. Chem. Chem. Phys. **15**, 9752 (2013).

[8] Y. Duan, D. Luebke, and H. W. Pennline, Efficient theoretical screening of solid sorbents for CO_2 capture applications, Int. J. Clean Coal Energy **01**, 1 (2012).

[9] Y. Duan, H. Pfeiffer, B. Li, I. C. Romero-Ibarra, D. C. Sorescu, D. R. Luebke, and J. W. Halley, CO_2 capture properties of lithium silicates with different ratios of Li_2O/SiO_2: An *ab initio* thermodynamic and experimental approach, Phys. Chem. Chem. Phys. **15**, 13538 (2013).

[10] Y. Duan, Electronic structural and phonon properties of lithium zirconates and their capabilities of CO_2 capture: A first-principle density functional approach, J. Renew. Sustain. Energy **3**, 013102 (2011).

[11] Y. Duan, A first-principles density functional theory study of the electronic structural and thermodynamic properties of M_2ZrO_3 and M_2CO_3 (M = Na,K) and their capabilities for CO_2 capture, J. Renew. Sustain. Energy **4**, 013109 (2012).

[12] Y. Duan and K. Parlinski, Density functional theory study of the structural, electronic, lattice dynamical, and thermodynamic properties of Li_4SiO_4 and its capability for CO_2 capture, Phys. Rev. B **84**, 104113 (2011).

[13] Y. Duan and D. C. Sorescu, Density functional theory studies of the structural, electronic, and phonon properties of Li_2O and Li_2CO_3: Application to CO_2 capture reaction, Phys. Rev. B **79**, 014301 (2009).

[14] Y. Duan and D. C. Sorescu, CO_2 capture properties of alkaline earth metal oxides and hydroxides: A combined density functional theory and lattice phonon dynamics study, J. Chem. Phys. **133**, 074508 (2010).

[15] K. L. Zhang, X. H. S. Li, Y. Duan, D. L. King, P. Singh, and L. Y. Li, Roles of double salt formation and $NaNO_3$ in Na_2CO_3-promoted MgO absorbent for intermediate temperature CO_2 removal, Int. J. Greenhouse Gas Contr. **12**, 351 (2013).

[16] J. L. Chi, L. F. Zhao, B. Wang, Z. Li, Y. H. Xiao, and Y. Duan, Thermodynamic performance assessment and comparison of IGCC with solid cycling process for CO_2 capture at high and medium temperatures, Int. J. Hydrogen Energy **39**, 6479 (2014).

[17] K. L. Zhang, X. H. S. Li, W. Z. Li, A. Rohatgi, Y. Duan, P. Singh, L. Y. Li, and D. L. King, Phase transfer-catalyzed fast CO_2 absorption by MgO-based absorbents with high cycling capacity, Adv. Mater. Interfaces **1**, 1400030 (2014).

[18] G. Pannocchia, M. Puccini, M. Seggiani, and S. Vitolo, Experimental and modeling studies on high-temperature capture of CO_2 using lithium zirconate based sorbents, Ind. Eng. Chem. Res. **46**, 6696 (2007).

[19] K. Nakagawa and T. Ohashi, A novel method of CO_2 capture from high temperature gases, J. Electrochem. Soc. **145**, 1344 (1998).

[20] K. Nakagawa and T. Ohashi, A reversible change between lithium zirconate and zirconia in molten carbonate, Electrochemistry **67**, 618 (1999).

[21] K. Essaki, K. Nakagawa, and M. Kato, Acceleration effect of ternary carbonate on CO_2 absorption rate in lithium zirconate powder, J. Ceram. Soc. Jpn. **109**, 829 (2001).

[22] K. Essaki, K. Nakagawa, M. Kato, and H. Uemoto, CO_2 absorption by lithium silicate at room temperature, J. Chem. Eng. Jpn. **37**, 772 (2004).

[23] K. Essaki, M. Kato, and H. Uemoto, Influence of temperature and CO_2 concentration on the CO_2 absorption properties of lithium silicate pellets, J. Mater. Sci. **40**, 5017 (2005).

[24] K. Essaki, M. Kato, and K. Nakagawa, CO_2 removal at high temperature using packed bed of lithium silicate pellets, J. Ceram. Soc. Jpn. **114**, 739 (2006).

[25] D. J. Fauth, E. A. Frommell, J. S. Hoffman, R. P. Reasbeck, and H. W. Pennline, Eutectic salt promoted lithium zirconate: Novel high temperature sorbent for CO_2 capture, Fuel Process. Technol. **86**, 1503 (2005).

[26] J. Ida and Y. S. Lin, Mechanism of high-temperature CO_2 sorption on lithium zirconate, Environ. Sci. Technol. **37**, 1999 (2003).

[27] J. Ida, R. T. Xiong, and Y. S. Lin, Synthesis and CO_2 sorption properties of pure and modified lithium zirconate, Sep. Purif. Technol. **36**, 41 (2004).

[28] E. Ochoa-Fernandez, M. Ronning, T. Grande, and D. Chen, Nanocrystalline lithium zirconate with improved kinetics for high-temperature CO_2 capture, Chem. Mater. **18**, 1383 (2006).

[29] H. Pfeiffer, E. Lima, and P. Bosch, Lithium-sodium metazirconate solid solutions, $Li_{2-x}Na_xZrO_3$ ($0 <= x <= 2$): A hierarchical architecture, Chem. Mater. **18**, 2642 (2006).

[30] H. Pfeiffer, C. Vazquez, V. H. Lara, and P. Bosch, Thermal behavior and CO_2 absorption of $Li_{2-x}Na_xZrO_3$ solid solutions, Chem. Mater. **19**, 922 (2007).

[31] H. K. Rusten, E. Ochoa-Fernandez, D. Chen, and H. A. Jakobsen, Numerical investigation of sorption enhanced

steam methane reforming using Li_2ZrO_3 as CO_2-acceptor, Ind. Eng. Chem. Res. **46**, 4435 (2007).

[32] Y. J. Wang, L. Qi, and W. J. Jiang, Effect of Na-doping on properties of lithium zirconate as CO_2-absorbent, Chinese J. Inorg. Chem. **22**, 1118 (2006).

[33] T. J. Zhao, E. Ochoa-Fernandez, M. Ronning, and D. Chen, Preparation and high-temperature CO_2 capture properties of nanocrystalline Na_2ZrO_3, Chem. Mater. **19**, 3294 (2007).

[34] M. Y. Veliz-Enriquez, G. Gonzalez, and H. Pfeiffer, Synthesis and CO_2 capture evaluation of $Li_{2-x}K_xZrO_3$ solid solutions and crystal structure of a new lithium-potassium zirconate phase, J. Solid State Chem. **180**, 2485 (2007).

[35] A. Lopez-Ortiz, N. G. P. Rivera, A. R. Rojas, and D. L. Gutierrez, Novel carbon dioxide solid acceptors using sodium containing oxides, Sep. Sci. Technol. **39**, 3559 (2005).

[36] E. Ochoa-Fernndez, M. Ronning, X. Yu, T. Grande, and D. Chen, Compositional effects of nanocrystalline lithium zirconate on its CO_2 capture properties, Ind. Eng. Chem. Res. **47**, 434 (2008).

[37] E. Ochoa-Fernandez, T. J. Zhao, M. Ronning, and D. Chen, Effects of steam addition on the properties of high temperature ceramic CO_2 acceptors, J. Environ. Eng. **135**, 397 (2009).

[38] A. Sandoval-Diaz and H. Pfeiffer, Effects of potassium doping on the composition, structure and carbon dioxide chemisorption of Na_2ZrO_3, Rev. Mex. Fis. **54**, 65 (2008).

[39] V. G. Velderrain, D. B. Jimenez, D. L. Gutierrez, D. D. Vigil, J. S. Gutierrez, A. L. Ortiz, and V. Collins-Martinez, Li promoted sodium zirconates as high temperature Absorbent, J. New Mater. Electrochem. Sys. **13**, 295 (2010).

[40] Y. Duan, Electronic, structural, phonon dynamical, and CO_2 capture properties of Li$M$$ZrO_3$ (M = Na,K) by *ab initio* thermodynamic investigation, ScienceJet **3**, 56 (2014).

[41] G. Kresse and J. Hafner, *Ab initio* molecular-dynamics for liquid-metals, Phys. Rev. B **47**, 558 (1993).

[42] G. Kresse and J. Furthmuller, Efficient iterative schemes for *Ab initio* total-energy calculations using a plane-wave basis set, Phys. Rev. B **54**, 11169 (1996).

[43] J. P. Perdew and Y. Wang, Accurate and simple analytic representation of the electron-gas correlation-energy, Phys. Rev. B **45**, 13244 (1992).

[44] Y. Duan, Electronic properties and stabilities of bulk and low-index surfaces of SnO in comparison with SnO_2: A first-principle density functional approach with an empirical correction of van der Waals interactions, Phys. Rev. B **77**, 045332 (2008).

[45] H. J. Monkhorst and J. D. Pack, Special points for Brillouin-zone integrations, Phys. Rev. B **13**, 5188 (1976).

[46] C. J. Bradley and A. P. Cracknell, *The Mathematical Theory of Symmetry in Solids* (Clarendon, Oxford, 1972).

[47] Y. Duan, K. Zhang, X. S. Li, D. L. King, B. Li, L. Zhao, and Y. Xiao, *Ab initio* thermodynamic study of the CO_2 capture properties of M_2CO_3 (M = Na,K)- and $CaCO_3$-promoted MgO sorbents towards forming double salts, Aerosol Air Qual. Res. **14**, 470 (2014).

[48] S. Cristol, J. F. Paul, E. Payen, D. Bougeard, S. Clemendot, and F. Hutschka, Theoretical study of the MoS_2 (100) surface: A chemical potential analysis of sulfur and hydrogen coverage. 2. Effect of the total pressure on surface stability, J. Phys. Chem. B **106**, 5659 (2002).

[49] J. H. Wang and M. Liu, Surface regeneration of sulfur-poisoned Ni surfaces under SOFC operation conditions predicted by first-principles-based thermodynamic calculations, J. Power Sources **176**, 23 (2008).

[50] R. G. Mortimer, *Physical Chemistry* (Academic, New York, 2000).

[51] M. Sternik and K. Parlinski, Free-energy calculations for the cubic ZrO_2 crystal as an example of a system with a soft mode, J. Chem. Phys. **123**, 204708 (2005).

[52] K. Parlinski, computer code PHONON (2010).

[53] K. Parlinski, Z. Q. Li, and Y. Kawazoe, First-Principles Determination of the Soft Mode in Cubic ZrO_2, Phys. Rev. Lett. **78**, 4063 (1997).

[54] P. Kubelka and F. Munk, Z. Tech. Phys. **12**, 593 (1931).

[55] See Supplemental Material at http://link.aps.org/supplemental/10.1103/PhysRevApplied.3.044013 for the experimental diffuse reflectance data for Li- and K-substituted Na_2ZrO_3, and for the calculated electronic band structures, density of states, and phonon dispersions of $Na_{2-x}M_xZrO_3$ (M = Li,K, x = 1.0,1.5).

[56] T. J. Bastow, M. E. Hobday, M. E. Smith, and H. J. Whitfield, Structural characterization of Na_2ZrO_3, Solid State Nucl. Magn. Reson. **3**, 49 (1994).

[57] B. M. Gatehouse and D. J. Lloyd, Crystal structure of potassium metazirconate and potassium metastannate—K_2ZrO_2 and K_2SnO_3—oxides with 5-coordinate square-pyramidal zirconium (4) and tin (4), J. Chem. Soc. D, 727 (1969).

[58] B. M. Gatehouse and D. J. Lloyd, The crystal structure of potassium metazirconate, K_2ZrO_3, and its tin analogue, K_2SnO_3, J. Solid State Chem. **2**, 410 (1970).

[59] G. Lang, Z. Anorg. Allg. Chem. **276**, 77 (1954).

[60] G. Lang, Z. Anorg. Allg. Chem. **348**, 246 (1966).

[61] P. Sanchez-Camacho, I. C. Romero-Ibarra, Y. Duan, and H. Pfeiffer, Thermodynamic and kinetic analyses of the CO_2 chemisorption mechanism on Na_2TiO_3: Experimental and theoretical evidences, J. Phys. Chem. C **118**, 19822 (2014).

[62] Cost and Performance Baseline for Fossil Energy Plants, http://www.netl.doe.gov/energy-analyses/baseline_studies.html.

[63] J. D. Figueroa, T. Fout, S. Plasynski, H. McIlvried, and R. D. Srivastava, Advances in CO_2 capture technology: The US Department of Energy's carbon sequestration program, Int. J. Greenhouse Gas Contr. **2**, 9 (2008).